

1. Calibration of the WFC3 filters

In a recent study (O’Dell et al. 2013) of NGC 6720, the Ring Nebula, evidence was found for significant deviations of some WFC3 UVIS narrow-band filter calibration constants from the pre-launch determined values given in the WFC3 Instrument Handbook. Several observationally important diagnostic line ratios are significantly impacted by the filter calibrations in question. It is therefore of paramount importance to confirm the calibrations under a wider range of nebular excitation conditions. The Orion Nebula, M42, provides an excellent complement to NGC 6720 in this respect, since it is of lower ionization and temperature, allowing the calibration to be extended to smaller values of the emission line equivalent widths, where continuum contamination of the narrow band filters is greater. At the same time, extensive high-quality spectrophotometric data exists for this object, obtained by distinct teams, using multiple telescopes and instruments (for example, Mesa-Delgado et al. 2008; O’Dell & Harris 2010). This allows the true spectrum to be determined with a degree of precision and confidence that is impossible for other objects.

1.1. Filter count rates

Assume we have pipeline-calibrated WFC3 UVIS images, R_j , in distinct filters j , which are in units $[R_j] = \text{counts s}^{-1} \text{ pixel}^{-1}$. The effective collecting area of the telescope is $A_{\text{HST}} = \pi(120 \text{ cm})^2 = 45,239 \text{ cm}^2$ and the solid angle subtended by each pixel is $\Omega_{\text{pix}} = (0.03962'')^2 = 3.6895 \times 10^{-14} \text{ sr}$. The transmission profile of the filter is given by T_λ^j , which is the total fractional throughput, accounting for camera and detector efficiencies (and including the fractional area of the primary mirror that is obscured by the secondary).

A source is observed that has a wavelength-dependent intensity I_λ in surface brightness units: $[I_\lambda] = \text{erg s}^{-1} \text{ cm}^{-2} \text{ sr}^{-1} \text{ \AA}^{-1}$. The expected count rate from the source is

$$R_j = A_{\text{HST}} \Omega_{\text{pix}} \int_0^\infty \varepsilon_\lambda^{-1} I_\lambda T_\lambda^j d\lambda \quad [R_j] = \text{counts s}^{-1} \text{ pixel}^{-1}, \quad (1)$$

where $\varepsilon_\lambda = 10^8(hc/\lambda)$ is the photon energy with $[\varepsilon_\lambda] = \text{erg}$ and $[\lambda] = \text{\AA}$. If the peak value of the filter transmission profile is T_m^j , then the “rectangular width” of the profile is defined as

$$W_j = (T_m^j)^{-1} \int_0^\infty T_\lambda^j d\lambda \quad [W_j] = \text{\AA}. \quad (2)$$

For a filter whose pass-band does not contain any strong emission lines, we can assume that I_λ is a slowly varying function of λ , in which case it is convenient to define an average intensity over the filter passband:

$$\langle \lambda I_\lambda \rangle_j = \int_0^\infty \lambda I_\lambda T_\lambda^j d\lambda / \int_0^\infty T_\lambda^j d\lambda. \quad (3)$$

Hence, from equations (1–3) we may write the count rate in this case as

$$R_j = C_{\text{WFC3}} \langle \lambda I_\lambda \rangle_j T_m^j W_j, \quad (4)$$

where $C_{\text{WFC3}} = 10^{-8} A_{\text{HST}} \Omega_{\text{pix}} / (hc) = 0.0840241 \text{ counts cm}^2 \text{ sr erg}^{-1} \text{ \AA}^{-1} \text{ pixel}^{-1}$.

Next, consider a filter whose pass-band contains one or more narrow emission lines i , each with central wavelength λ_i and wavelength-integrated intensity I_i , plus a smoothly varying continuum I_λ^{cont} :

$$I_\lambda = I_\lambda^{\text{cont}} + \sum_{i=1,n} I_i \delta(\lambda - \lambda_i), \quad (5)$$

where δ denotes the Dirac delta function. The equivalent width, or EW, of each line is $-E_i$ with respect to its local continuum, where

$$E_i = I_i/I_\lambda^i \quad [E_i] = \text{\AA}, \quad (6)$$

and in which $I_\lambda^i \equiv I_\lambda^{\text{cont}}(\lambda = \lambda_i)$ is the continuum intensity at the line wavelength. The filter transmission at the line wavelength is denoted $T_i^j \equiv T_\lambda^j(\lambda = \lambda_i)$ and the color term $k_{j,i}$ is defined as the ratio of the mean continuum intensity in the filter to the continuum intensity at the line wavelength:

$$k_{j,i} \equiv \frac{\langle \lambda I_\lambda^{\text{cont}} \rangle_j}{\lambda_i I_\lambda^i}. \quad (7)$$

Note that $k_{j,i}$ will be very close to unity so long as the filter is narrow. It is also convenient to define an “effective width” of the filter with respect to the emission line:

$$\tilde{W}_{j,i} \equiv k_{j,i} \frac{T_m^j}{T_i^j} W_j. \quad (8)$$

From the foregoing, the count rate in this case is found to be

$$R_j = C_{\text{WFC3}} \langle \lambda I_\lambda^{\text{cont}} \rangle_j T_m^j W_j \left(1 + \sum_{i=1,n} E_i / \tilde{W}_{j,i} \right). \quad (9)$$

1.2. Filter Ratio Type I

We first consider finding the ratio between the count rate in a narrow filter ($j = N$) that contains a single emission line, given by equation (9) with $n = 1$, and the rate in a broader filter ($j = W$) that passes only continuum, given by equation (4). It is convenient to define a filter-to-filter continuum color:

$$k_{N,W} \equiv \frac{\langle \lambda I_\lambda^{\text{cont}} \rangle_N}{\langle \lambda I_\lambda^{\text{cont}} \rangle_W}, \quad (10)$$

such that the ratio is given by

$$\frac{R_N}{R_W} = k_{N,W} \frac{T_m^N W_N}{T_m^W W_W} \left(1 + \frac{E_i}{\tilde{W}_{N,i}} \right). \quad (11)$$

Note that the factor $E_i/\tilde{W}_{N,i}$ gives the relative importance of the line over the continuum in the narrow filter, and that the filter count ratio is a linear function of the line equivalent width.

1.3. Filter Ratio Type IIa

If the *same* emission line is present in the pass band of the wide filter as well as the narrow filter, then it is necessary to use equation (9) for both filters. However, in this case one commonly has $E_i \ll \tilde{W}_{W,i}$ and so it is sufficient to expand the ratio in powers of $E_i/\tilde{W}_{W,i}$:

$$\frac{R_N}{R_W} = k_{N,W} \frac{T_m^N W_N}{T_m^W W_W} \left(1 + \frac{E_i}{\tilde{W}_{N,i}} \right) \left(1 - \frac{E_i}{\tilde{W}_{W,i}} \right) + \mathcal{O} \left[\left(\frac{E_i}{\tilde{W}_{W,i}} \right)^2 \right]. \quad (12)$$

If only the term linear in $E_i/\tilde{W}_{W,i}$ is retained, the ratio becomes

$$\frac{R_N}{R_W} \simeq k_{N,W} \frac{T_m^N W_N}{T_m^W W_W} \left(1 + E_i \left(\frac{1}{\tilde{W}_{N,i}} - \frac{1}{\tilde{W}_{W,i}} \right) - \frac{E_i^2}{\tilde{W}_{N,i} \tilde{W}_{W,i}} \right). \quad (13)$$

Thus the effect of a small “contamination” of the wide filter by the emission line is to reduce the slope of the relation between line equivalent width and filter ratio, and also to introduce a slight negative curvature for the highest equivalent widths.

1.4. Filter Ratio Type IIb

If the wide filter is contaminated by one or more *different* lines, i' , then similar considerations apply. But in this case, the shape of the EW–filter ratio relation is unaffected and the contamination is best accommodated by simply modifying the filter-to-filter color ratio to include the contribution of the contaminating lines:

$$\tilde{k}_{N,W} \equiv \frac{\langle \lambda I_\lambda^{\text{cont}} \rangle_N}{\langle \lambda I_\lambda \rangle_W} = k_{N,W} \left(1 + \sum_{i' \neq i} \frac{E_{i'}}{\tilde{W}_{W,i'}} \right)^{-1}. \quad (14)$$

The ratio then retains the same simple form as for Type I:

$$\frac{R_N}{R_W} = \tilde{k}_{N,W} \frac{T_m^N W_N}{T_m^W W_W} \left(1 + \frac{E_i}{\tilde{W}_{N,i}} \right). \quad (15)$$

Note that no series expansion has been made in this case, and the above expressions are formally valid for arbitrarily high $\sum E_{i'}/\tilde{W}_{W,i'}$. However, if $E_{i'} > \tilde{W}_{W,i'}$ for any particular line, then the variations in R_N/R_W may be driven by variations in $E_{i'}$ as much as by variations in E_i , in which case the apparent simplicity of equation (15) is illusory.

1.5. Filter Ratio Type III

Two lines in the same filter – *TODO*

1.6. Relative calibration within filter sets

In the following, all 3-figure IDs denote a particular filter, j . For example W_{547} for the rectangular width of filter F547M. On the other hand, all 4-figure IDs denote a particular emission line, i . For example E_{6583} for the equivalent width of [N II] $\lambda 6583$.

1.6.1. F658N, FQ575N, and F547M: [N II] nebular and auroral lines

The narrow-band filter F658N ($W_{658} \simeq 28 \text{ \AA}$) passes the strong nebular line [N II] $\lambda 6583$, which has an equivalent width of $E_{6583} = 200\text{--}400 \text{ \AA}$ in M42, rising to more than 3000 \AA in the the main ring of NGC 6720. The continuum contribution to the filter is therefore always small, of order 10% in M42 and < 1% in NGC 6720.

The even narrower quad filter FQ575N ($W_{575} \simeq 21 \text{ \AA}$) passes the relatively weak auroral line [N II] $\lambda 5755$, which has an equivalent width of $E_{5755} = 2\text{--}10 \text{ \AA}$ in M42, reaching values as high as 100 \AA in NGC 6720. We therefore expect a significant continuum contribution to the filter of 50–90% in M42 and $\sim 20\%$ in NGC 6720.

The medium-band filter F547M ($W_{547} \simeq 650 \text{ \AA}$) is dominated by continuum emission in lower excitation sources such as M42, where the total EW of emission lines in the filter is generally < 20 \AA , corresponding to a few percent of the filter flux. In

NGC 6720 on the other hand, [N II] $\lambda 5755$ and other lines such as [N I] $\lambda 5198, 5200$ and He II $\lambda 5411$ can sum to a total EW of 100–300 Å and contribute 15–30% of the total F547M flux.

The ratio R_{658}/R_{547} is therefore of Type IIa, so that if E_{6583} and $\tilde{k}_{658,547}$ can be measured independently from spectrophotometry for a sufficiently large range of E_{6583} , for which co-spatial WFC3 observations are available, then the filter constants can be determined graphically from the slope and intercept of the EW–ratio relation as follows:

$$\frac{R_{658}}{\tilde{k}_{658,547} R_{547}} = r_0(1 + q_1 E_{6583}), \quad (16)$$

where

$$r_0 = \frac{T_m^{658} W_{658}}{T_m^{547} W_{547}}, \quad q_1 = \frac{1}{\tilde{W}_{658,6583}}.$$

The ratio R_{575}/R_{547} is of Type IIab and should obey a relation:

$$\frac{R_{575}}{\tilde{k}_{575,547} R_{547}} = r_0 \left(1 + q_1 E_{5755} (1 - q_2 E_{5755}) \right) \quad (17)$$

where

$$r_0 = \frac{T_m^{575} W_{575}}{T_m^{547} W_{547}}, \quad q_1 = \frac{\tilde{W}_{547,5755} - \tilde{W}_{575,5755}}{\tilde{W}_{547,5755} \tilde{W}_{575,5755}}, \quad q_2 = \frac{1}{\tilde{W}_{547,5755} - \tilde{W}_{575,5755}}.$$

1.6.2. $F673N$, $FQ672N$, and $FQ674N$: [S II] nebular doublet

1.6.3. $FQ436N$, $FQ437N$, $F502N$, and $F547M$: $H\gamma$ and [O III] nebular and auroral lines

This is going to be the most challenging.

1.7. Absolute calibration

2. Raw filter comparison

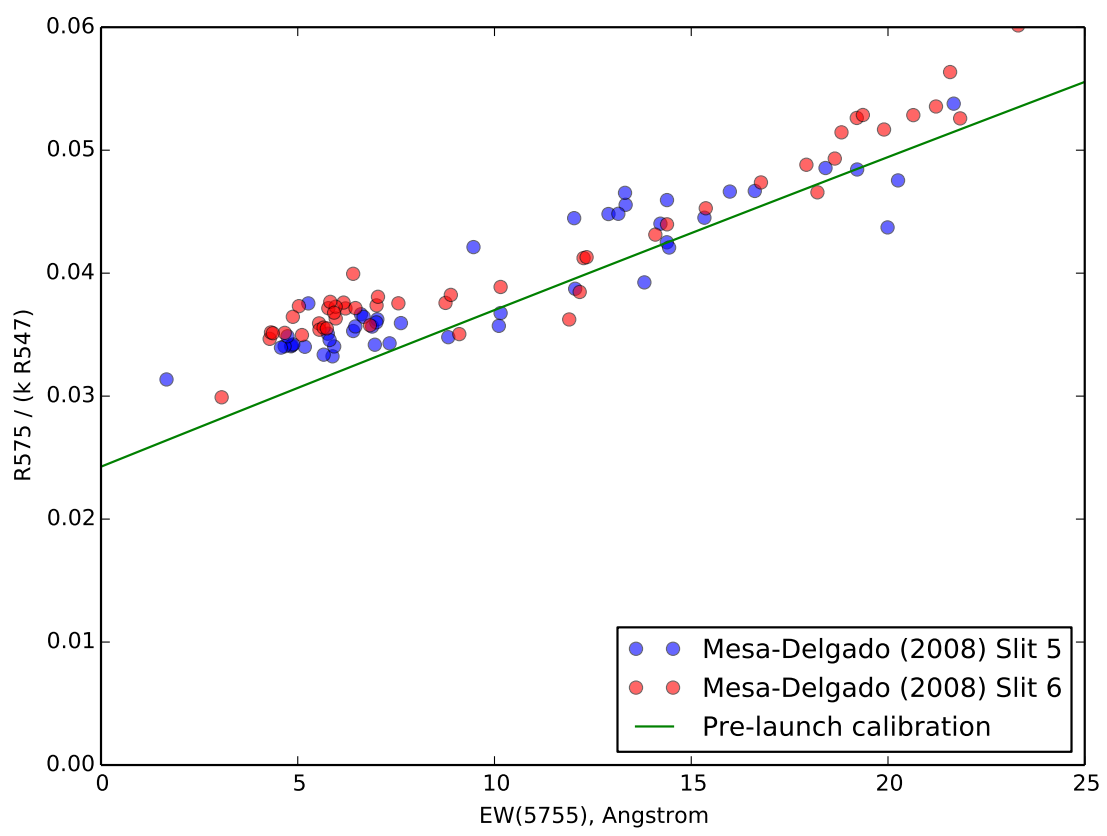
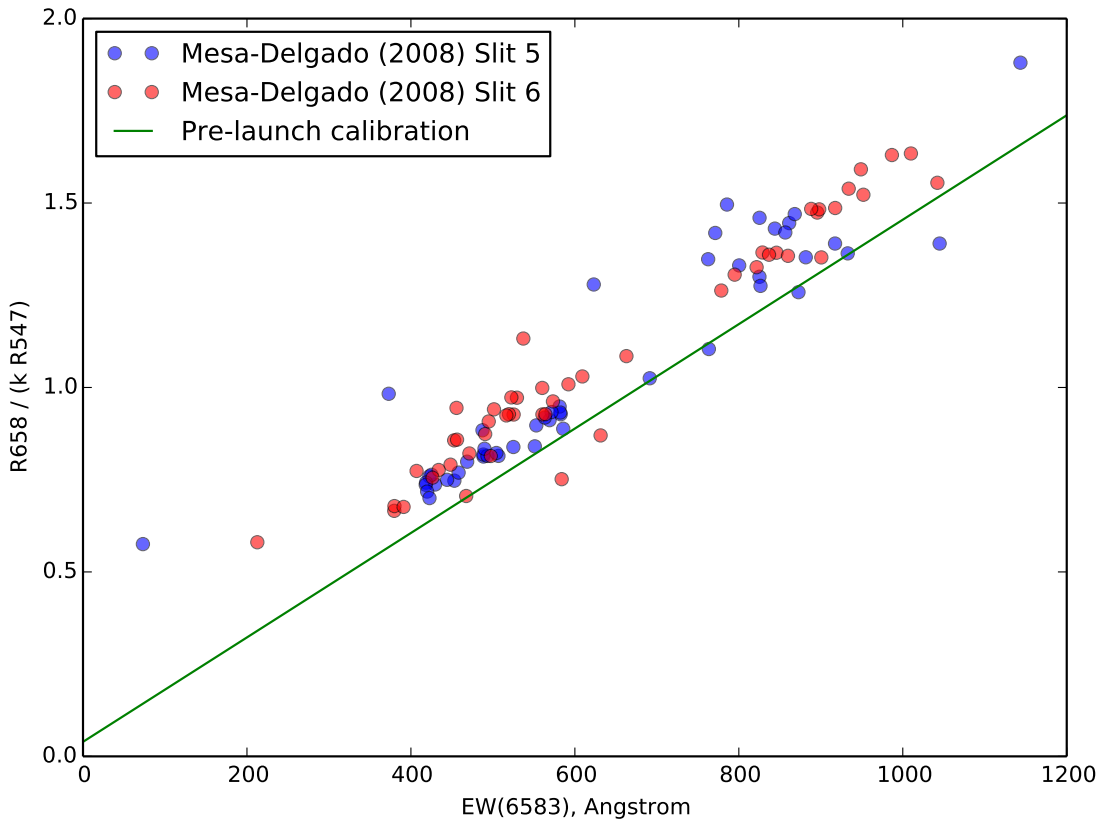
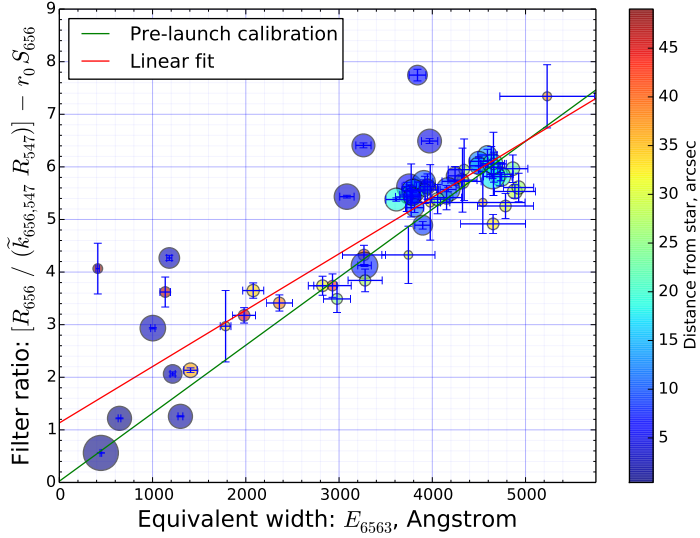
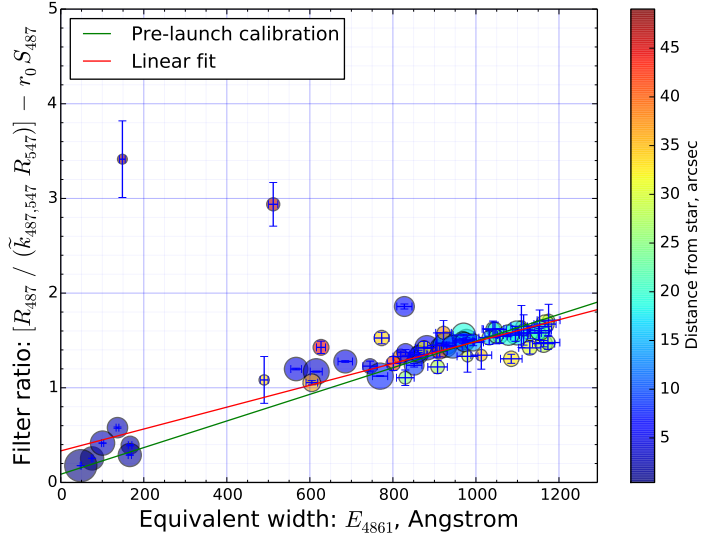


Fig. 1.— Preliminary calibration of 5755 and 6583

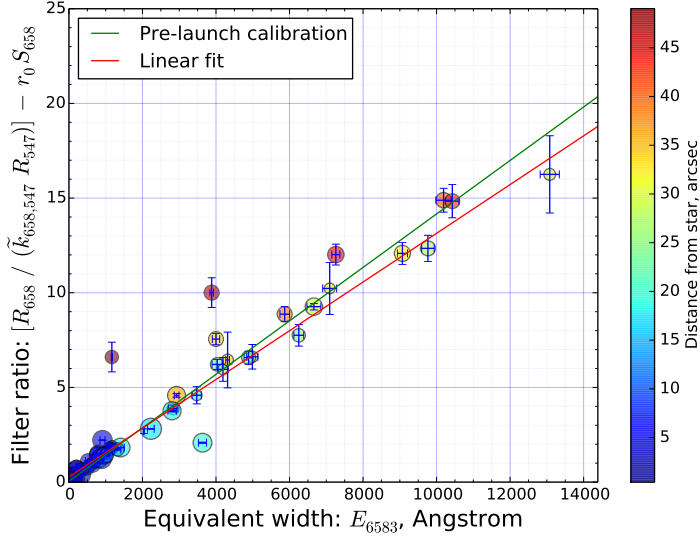
(a)

F656N: H α λ 6563

(b)

F486N: H β λ 4861

(c)

F658N: [N II] λ 6583

(d)

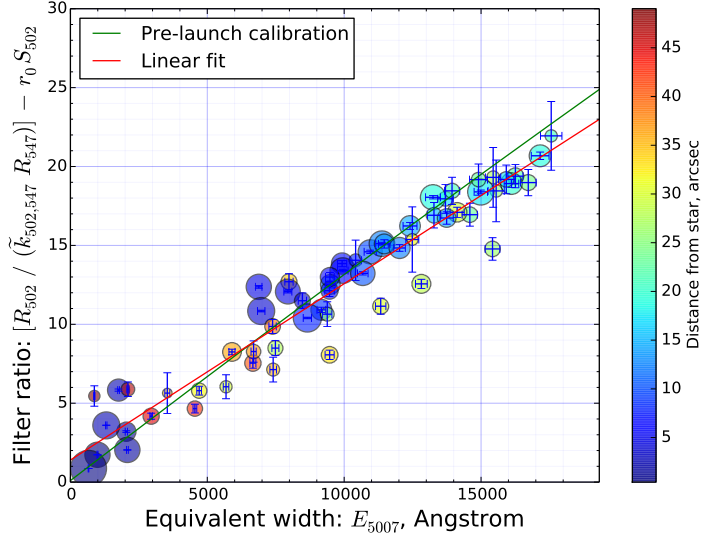
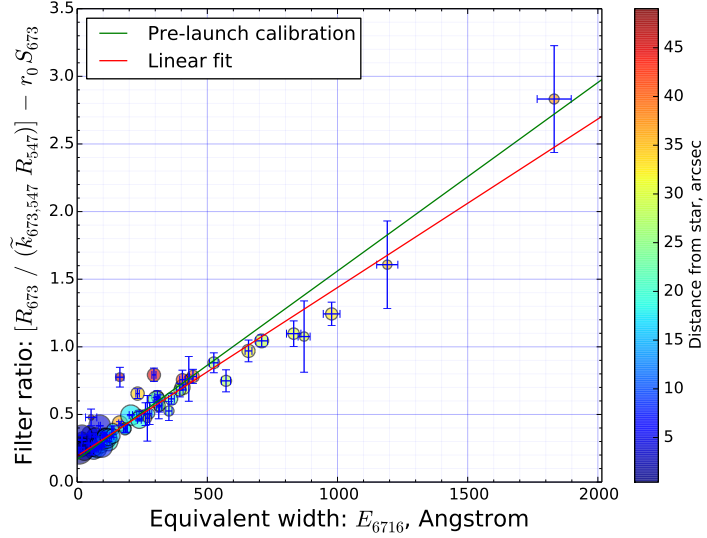
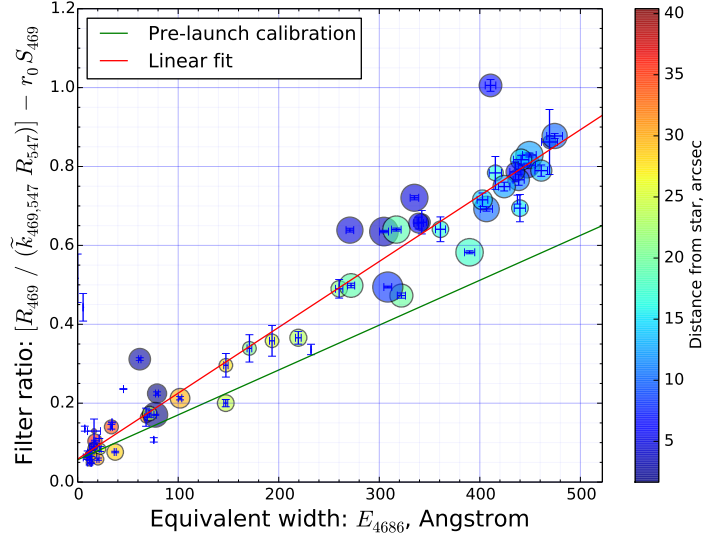
F502N: [O III] λ 5007

Fig. 2.— Strong lines versus continuum. Ring Nebula calibration. All are consistent with the pre-launch calibration.

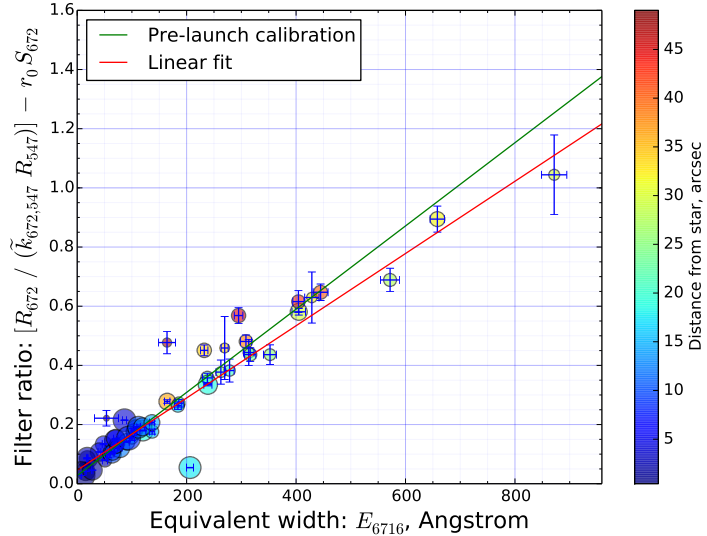
(a)

F673N: [S II] $\lambda 6716 + 31$ 

(b)

F469N: He II $\lambda 4686$ 

(c)

FQ672N: [S II] $\lambda 6716$ 

(d)

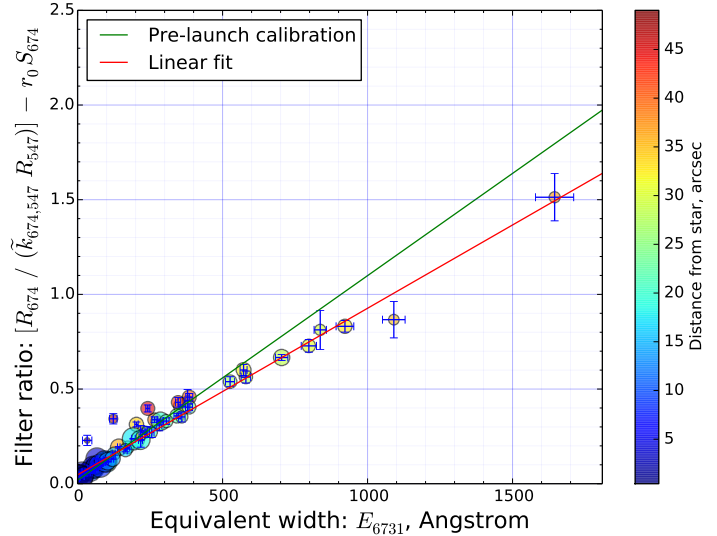
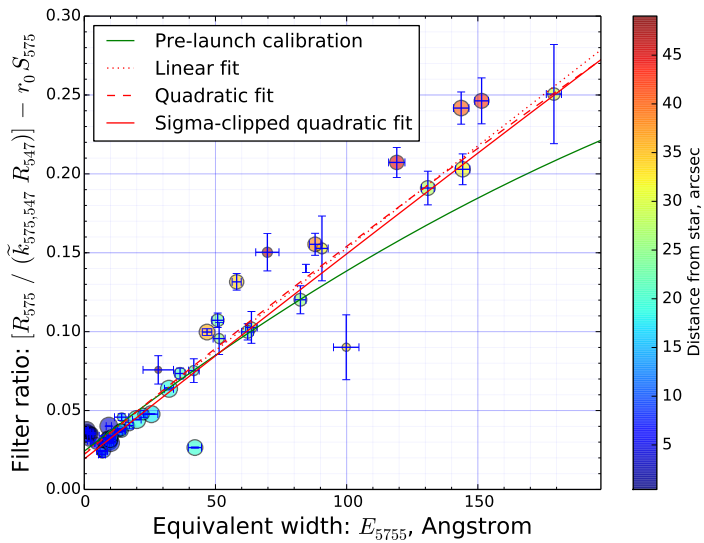
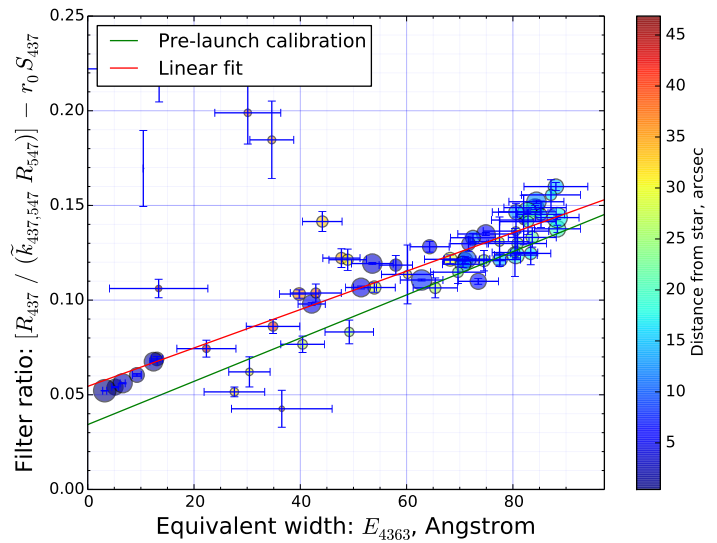
FQ674N: [S II] $\lambda 6731$ 

Fig. 3.— Medium lines versus continuum. Ring Nebula calibration. (a) Broad [S II] nebular filter. Note that I need to include the EW of both lines in the x-axis. (b) He II filter. I still need to correct for the [Ar IV] and He I but that should only be a 10% effect. (c) and (d) Narrow [S II] nebular filters. There is a significant deviation from the pre-launch calibration for FQ674N.

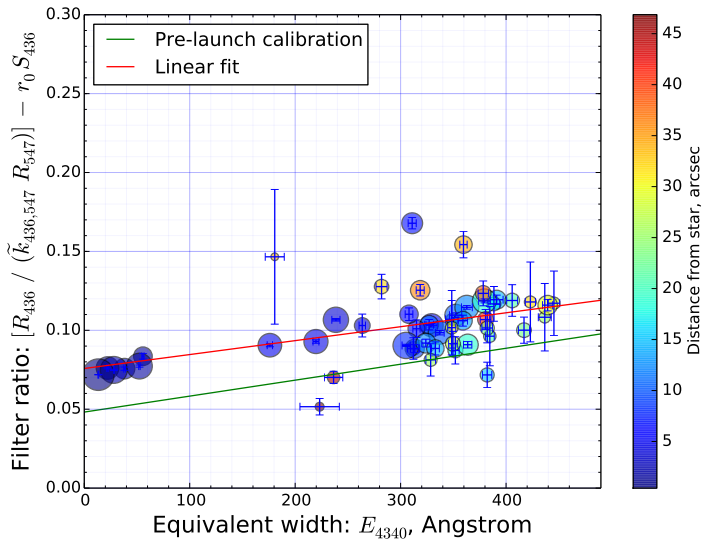
(a)

FQ575N: [N II] $\lambda 5755$ 

(b)

FQ437N: [O III] $\lambda 4363$ 

(c)

FQ436N: H γ $\lambda 4340$ 

(d)

Fig. 4.— Weak lines versus continuum. Ring Nebula calibration.

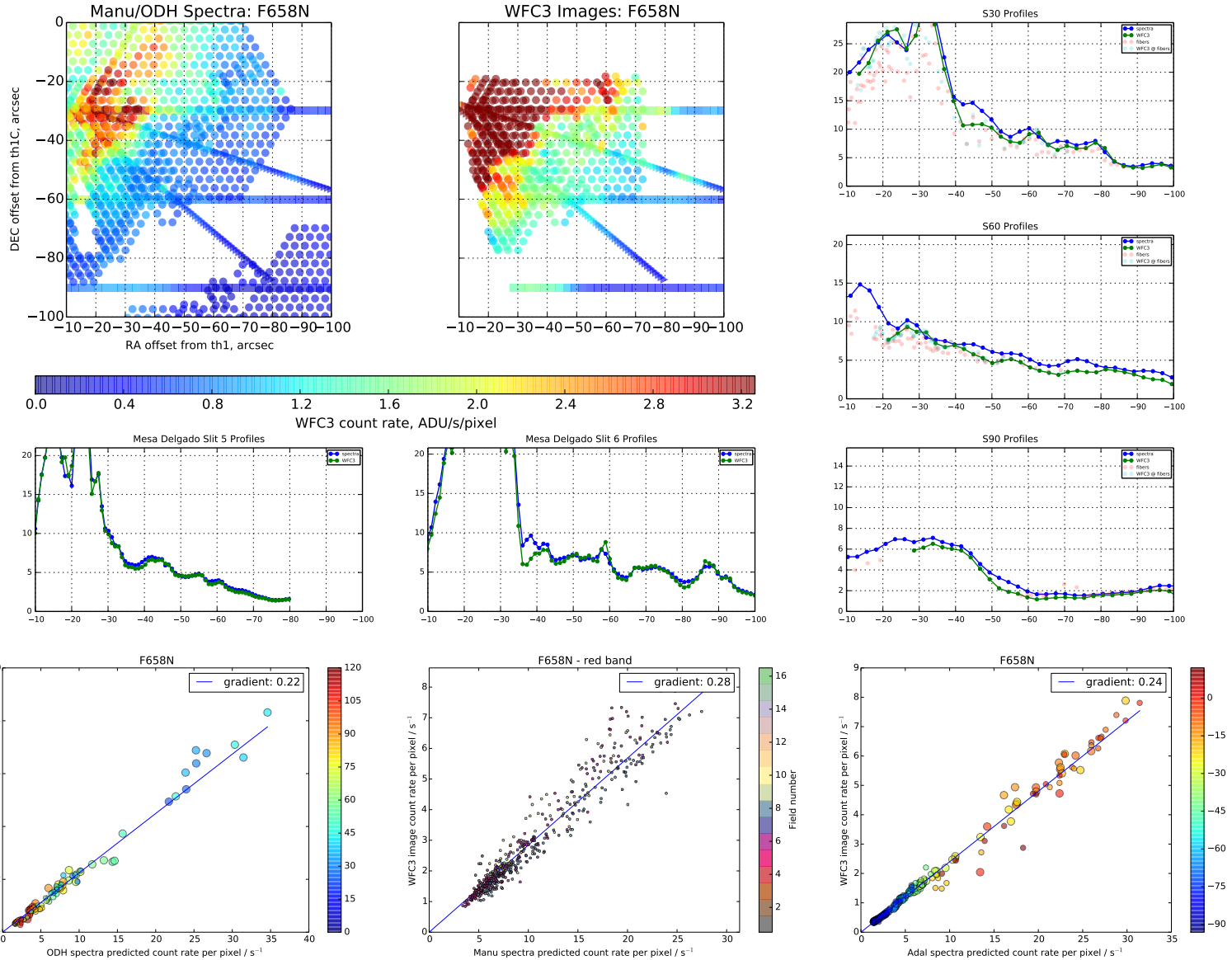


Fig. 5.— Orion Nebula raw filter comparison for F658N

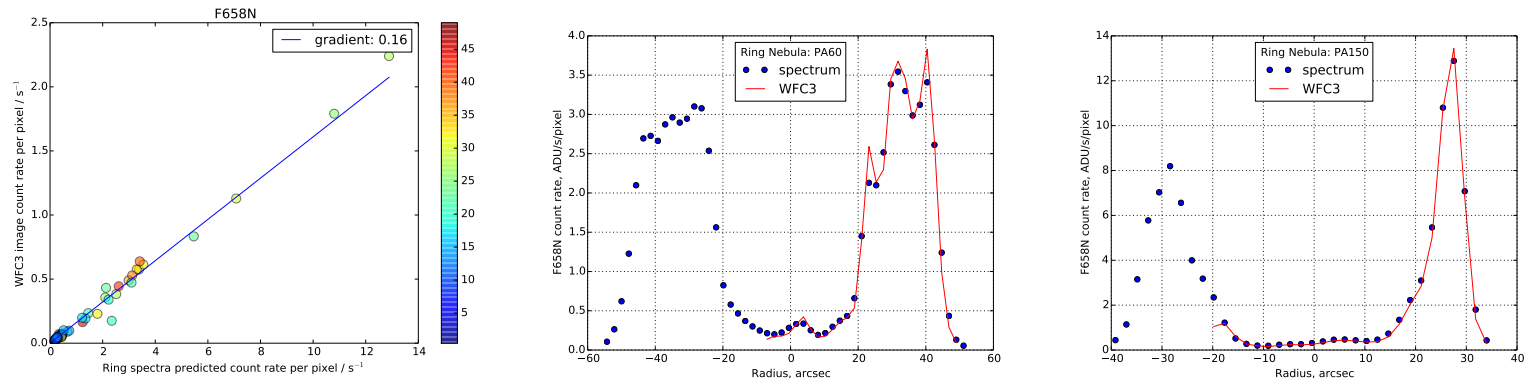


Fig. 6.— Ring Nebula raw filter comparison for F658N

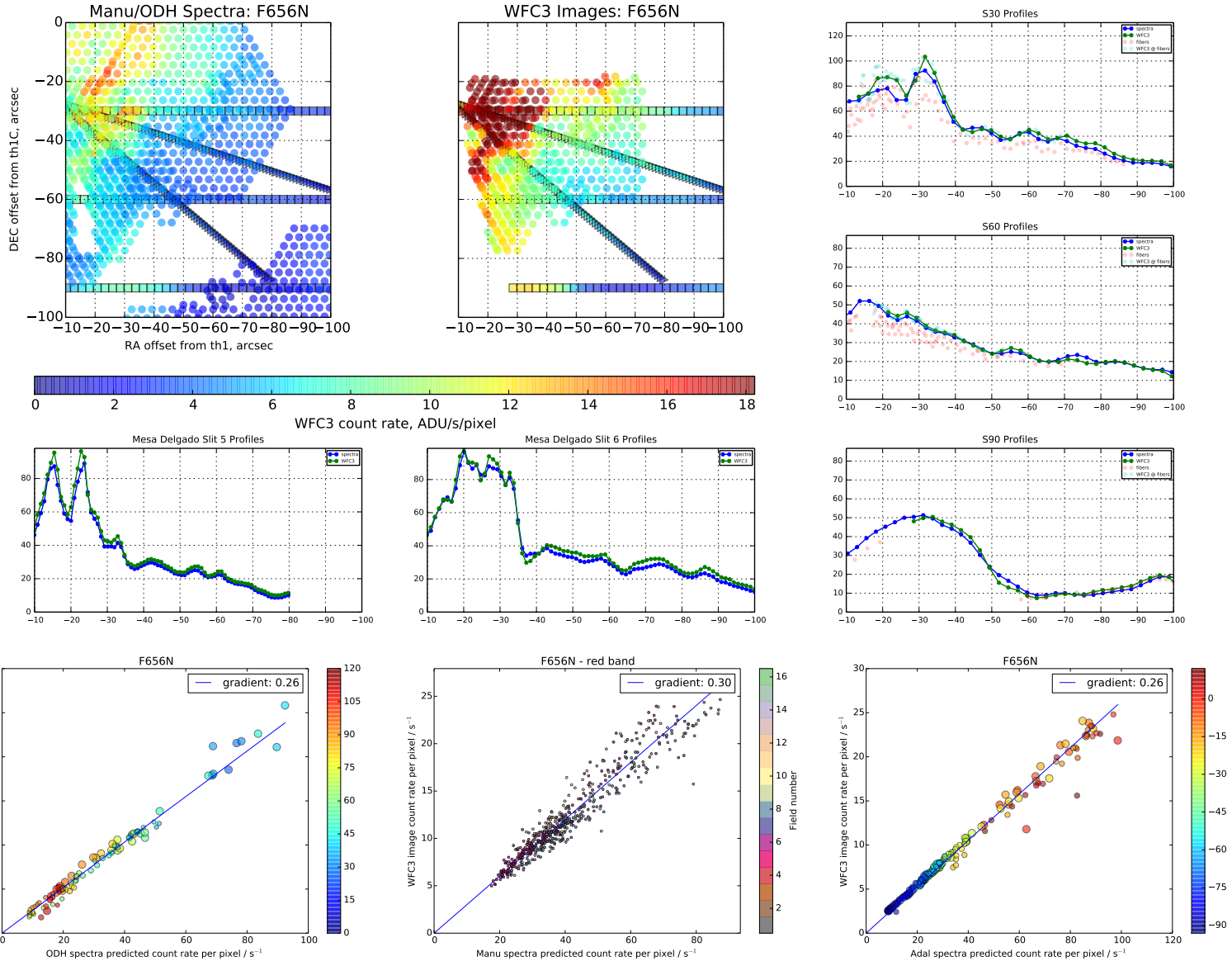


Fig. 7.— Orion Nebula raw filter comparison for F656N

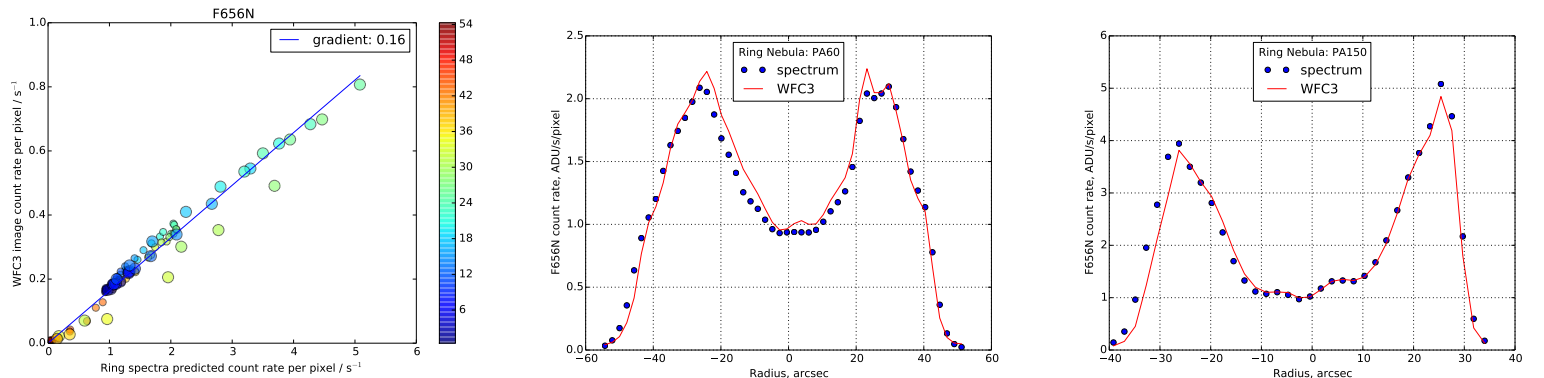


Fig. 8.— Ring Nebula raw filter comparison for F656N

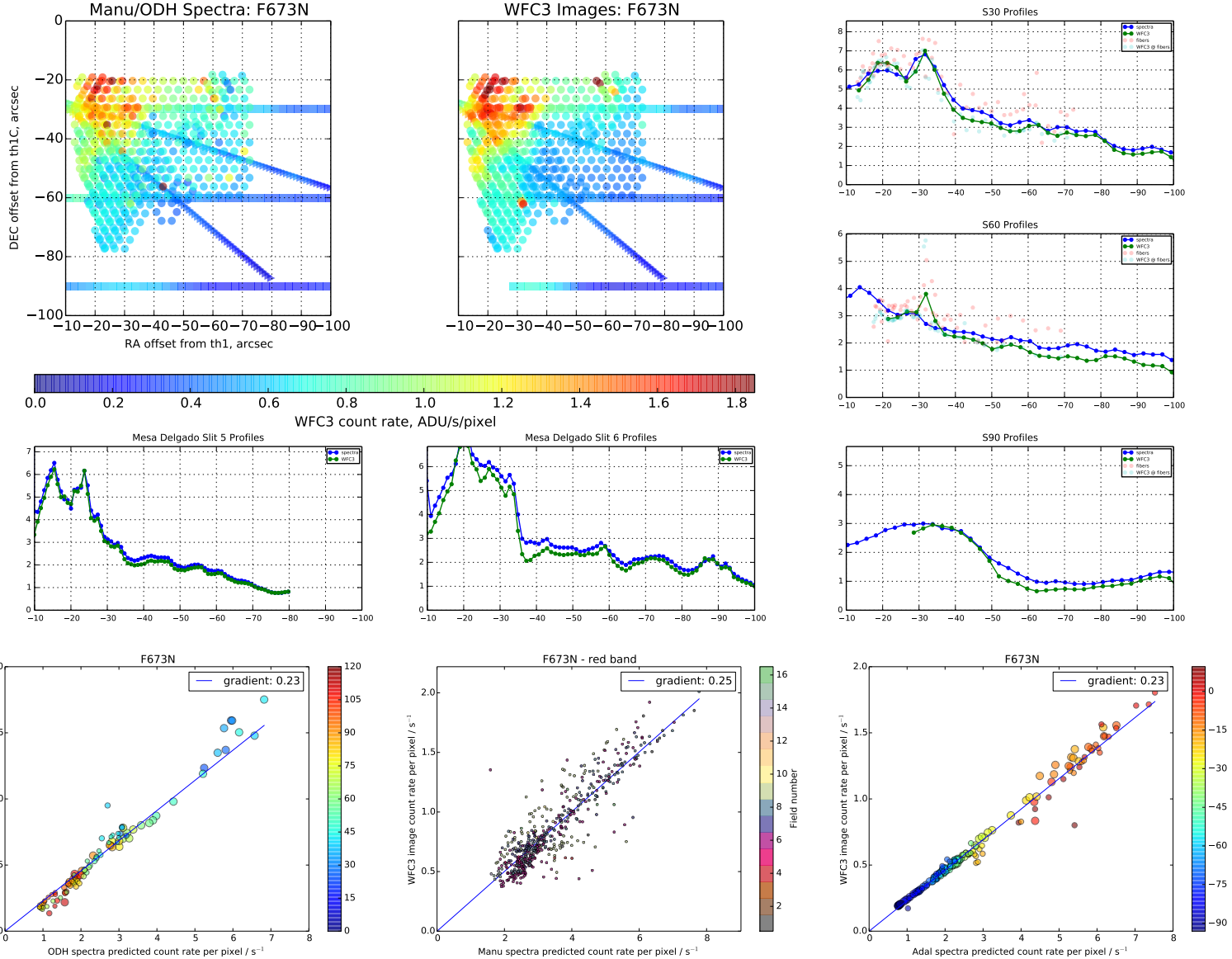


Fig. 9.— Orion Nebula raw filter comparison for F673N

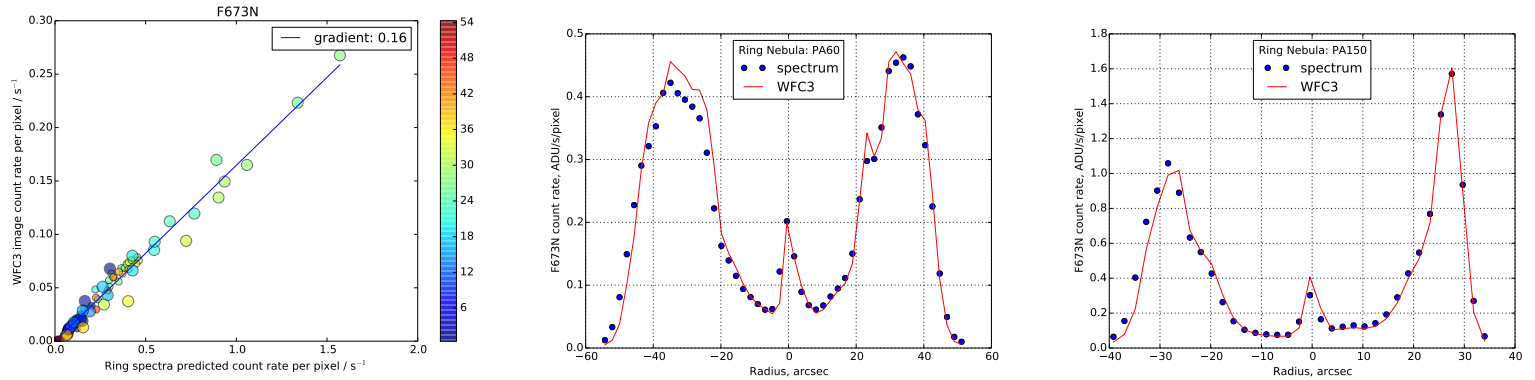


Fig. 10.— Ring Nebula raw filter comparison for F673N

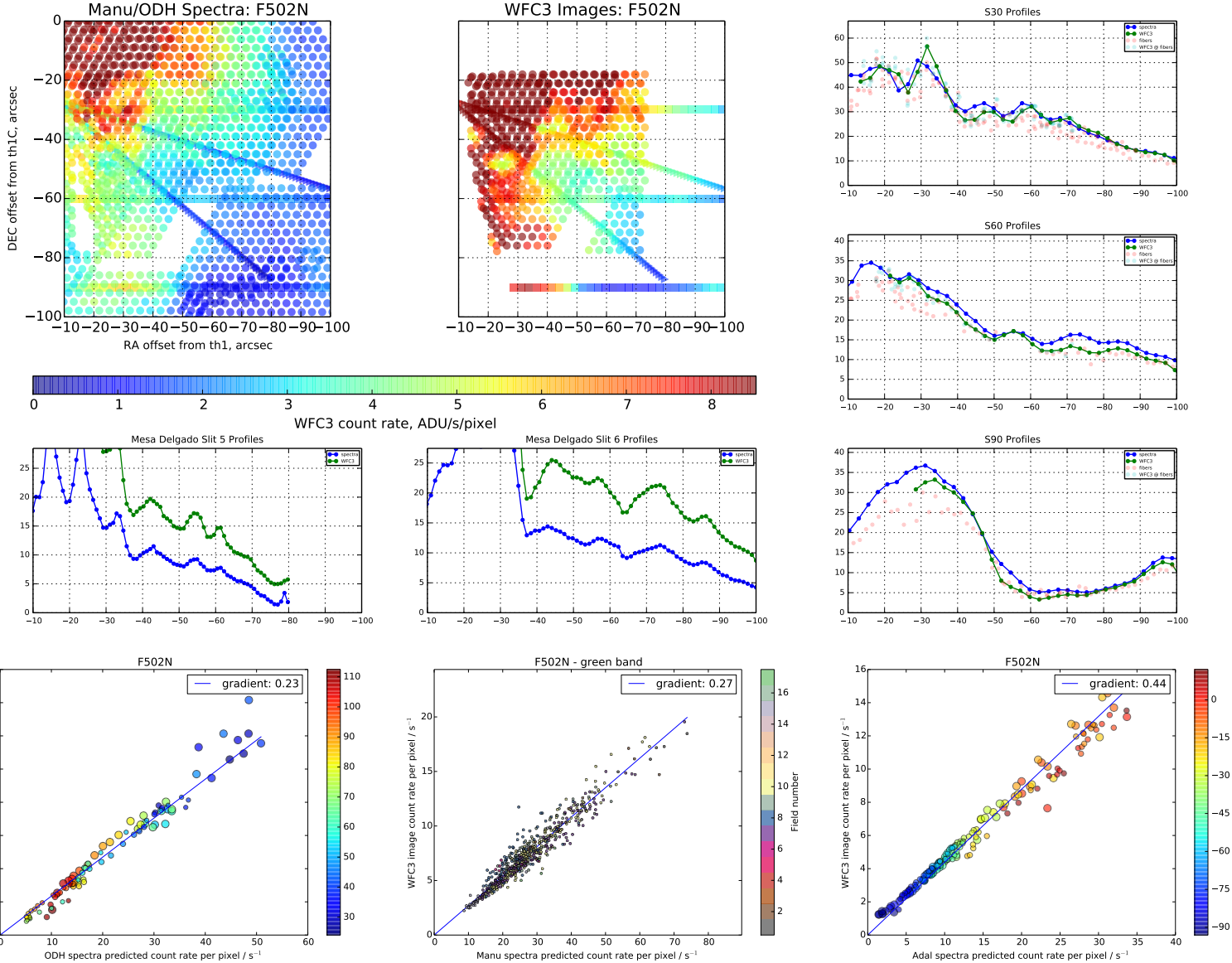


Fig. 11.— Orion Nebula raw filter comparison for F502N

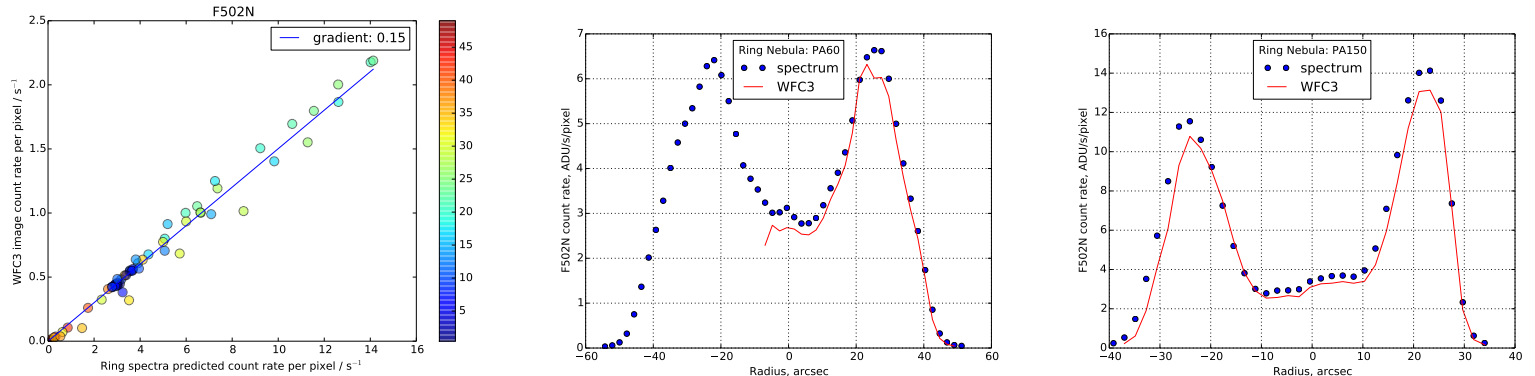


Fig. 12.— Ring Nebula raw filter comparison for F502N

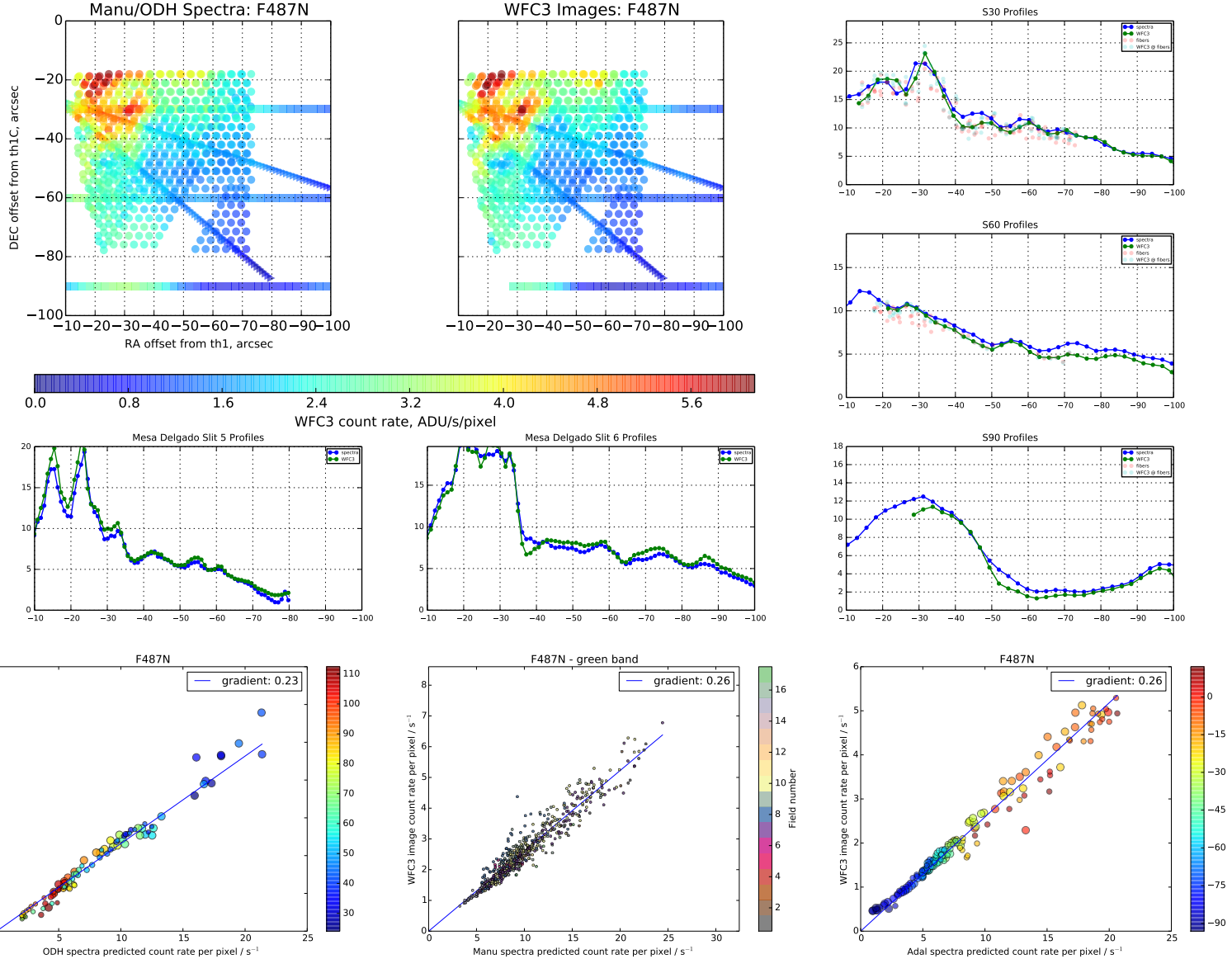


Fig. 13.— Orion Nebula raw filter comparison for F487N

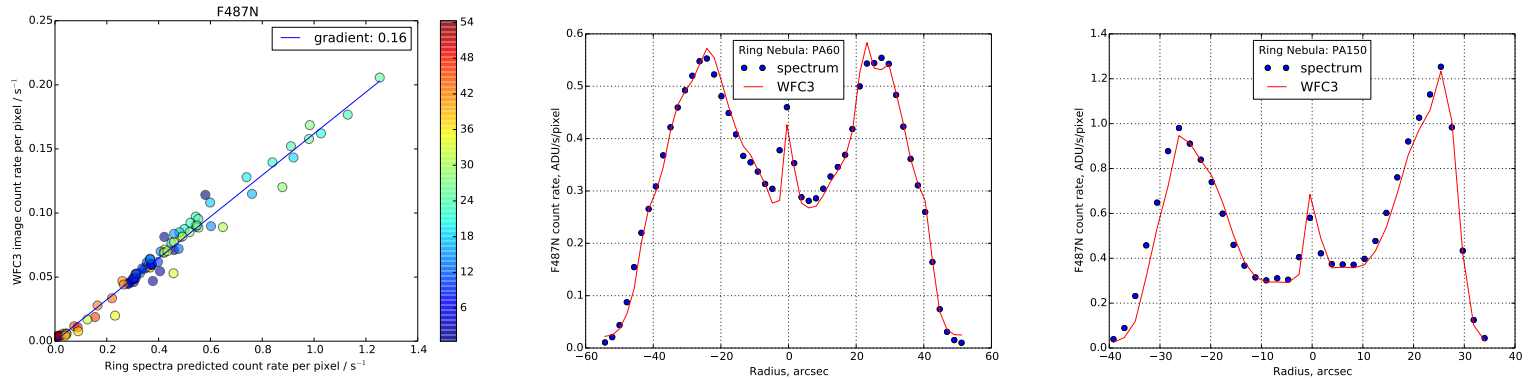


Fig. 14.— Ring Nebula raw filter comparison for F487N

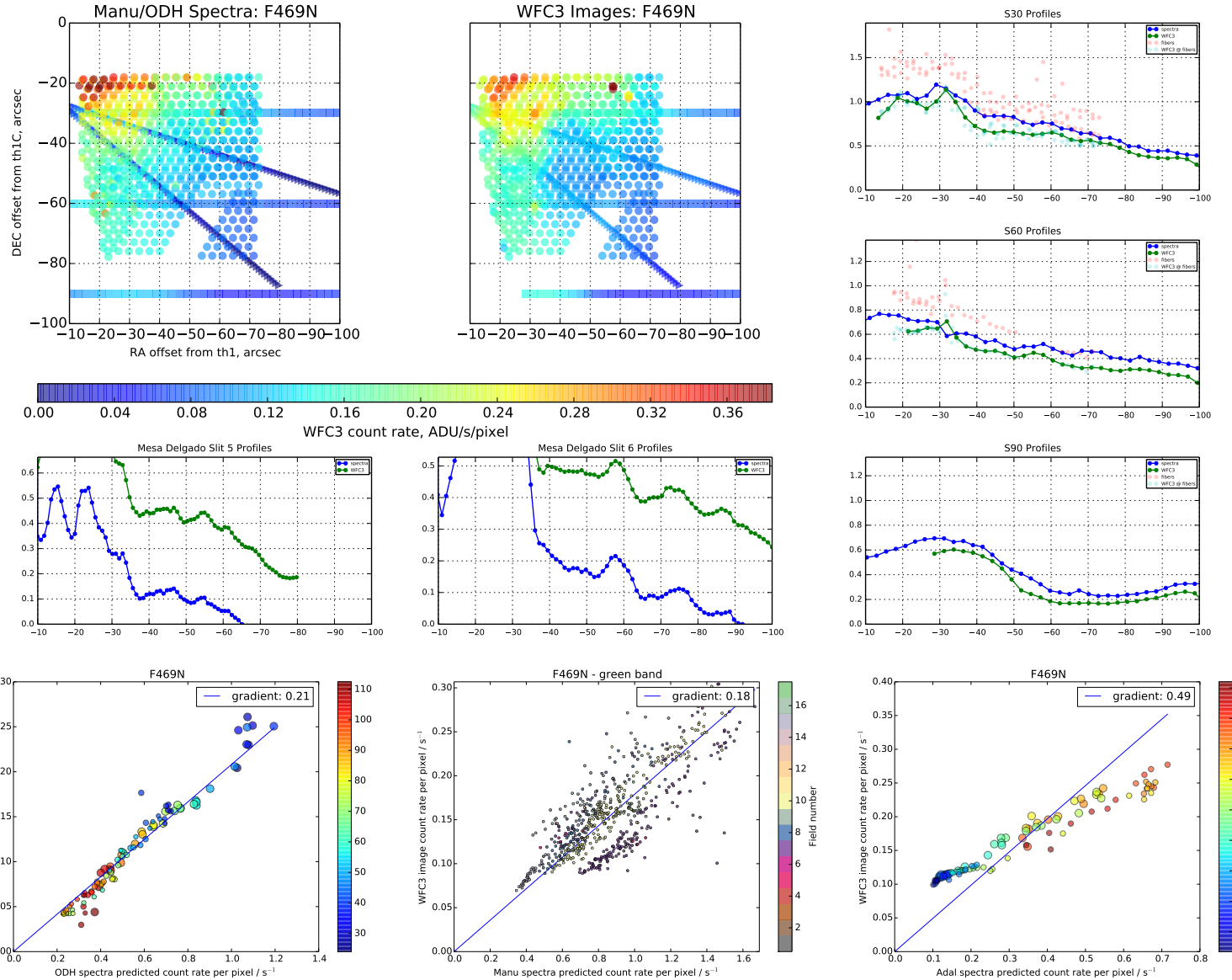


Fig. 15.— Orion Nebula raw filter comparison for F469N

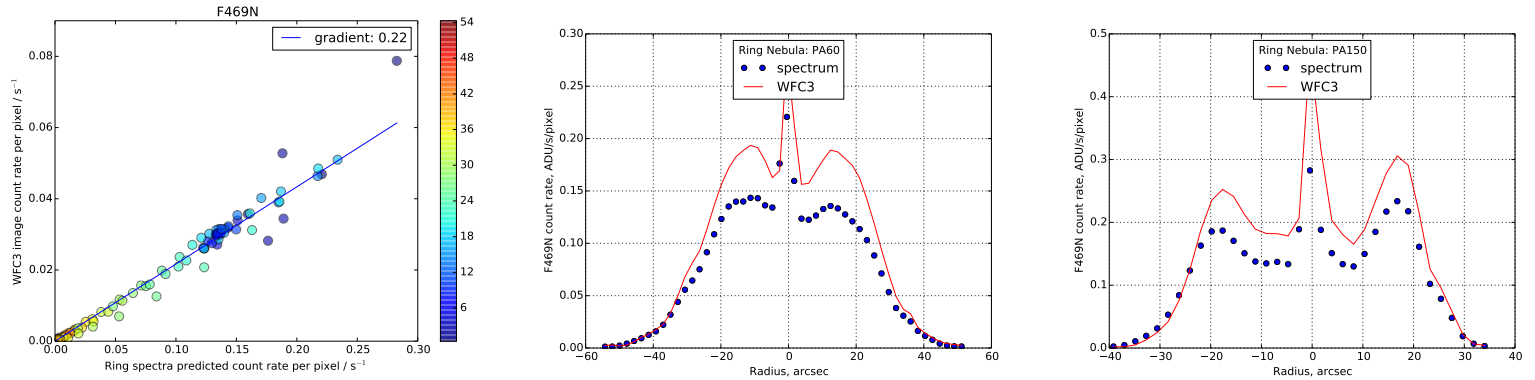


Fig. 16.— Ring Nebula raw filter comparison for F469N

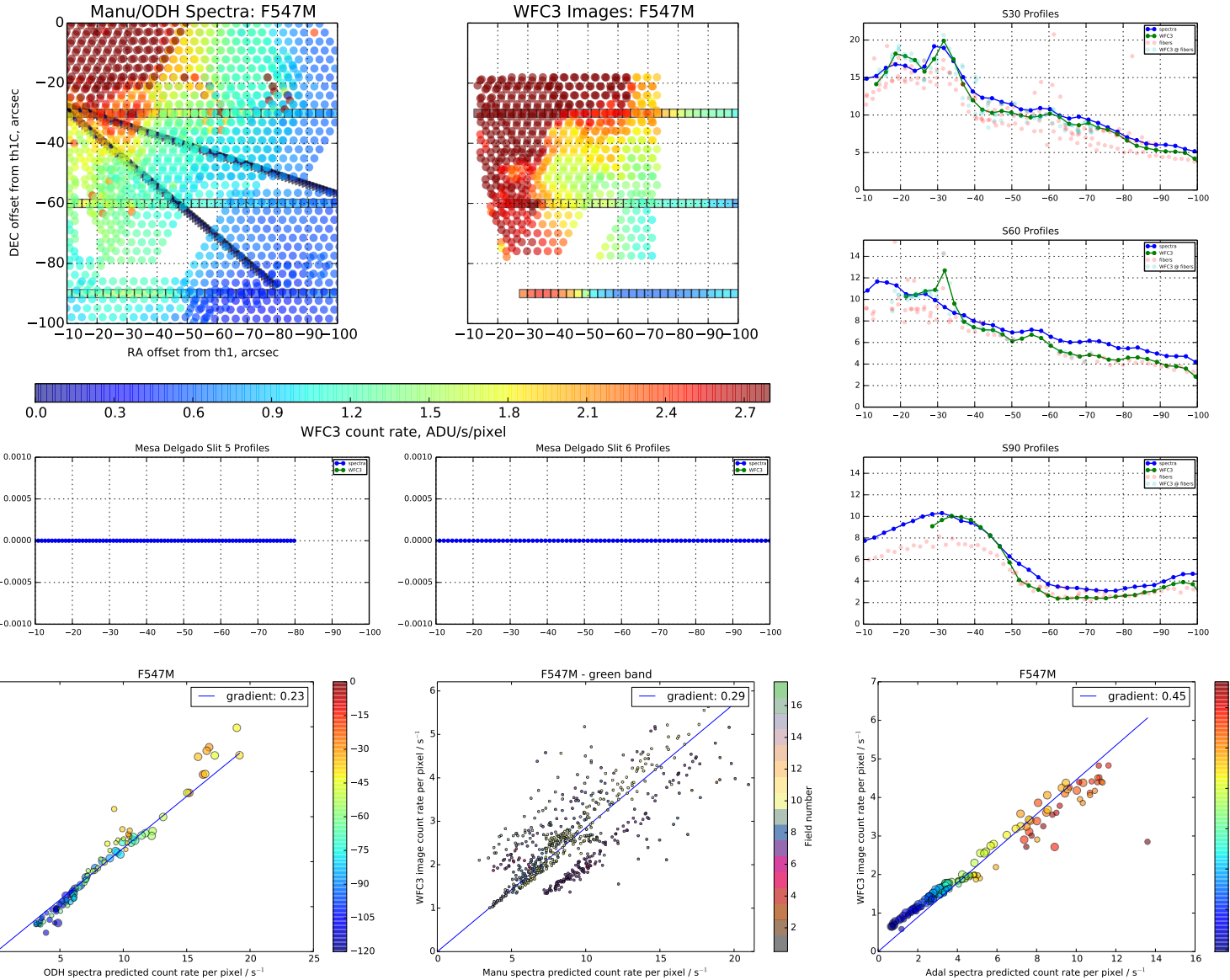


Fig. 17.— Orion Nebula raw filter comparison for F547M

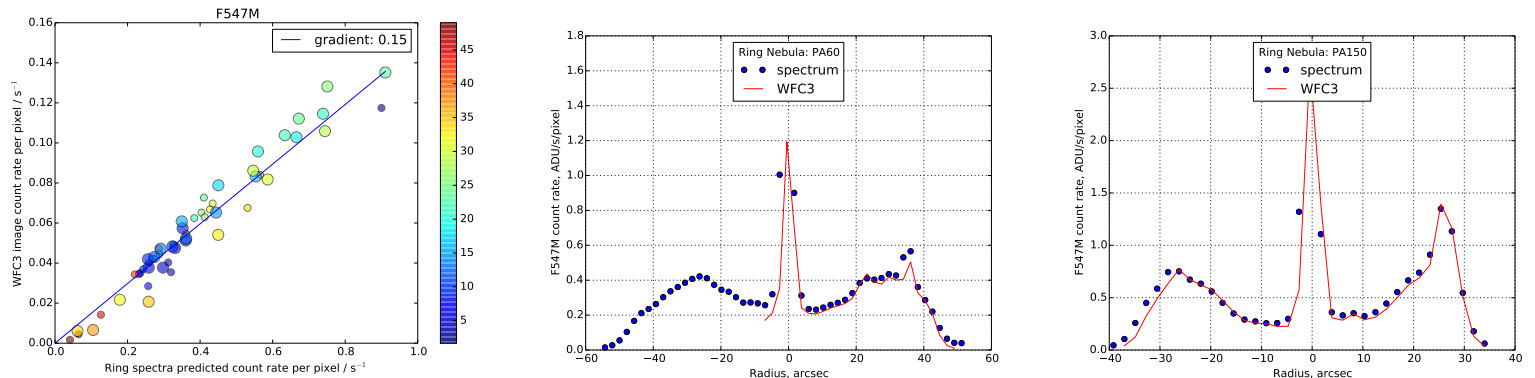


Fig. 18.— Ring Nebula raw filter comparison for F547M

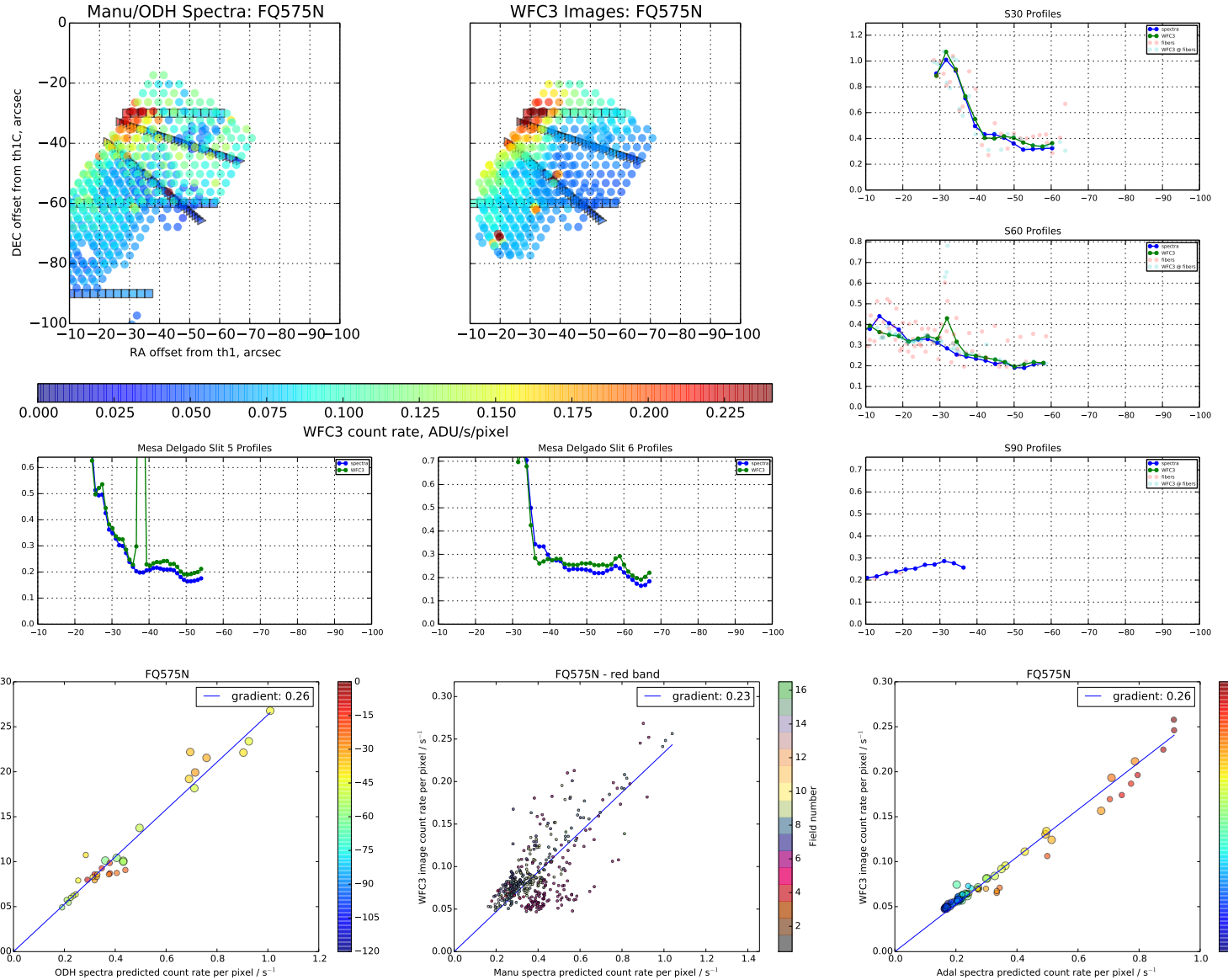


Fig. 19.— Orion Nebula raw filter comparison for FQ575N

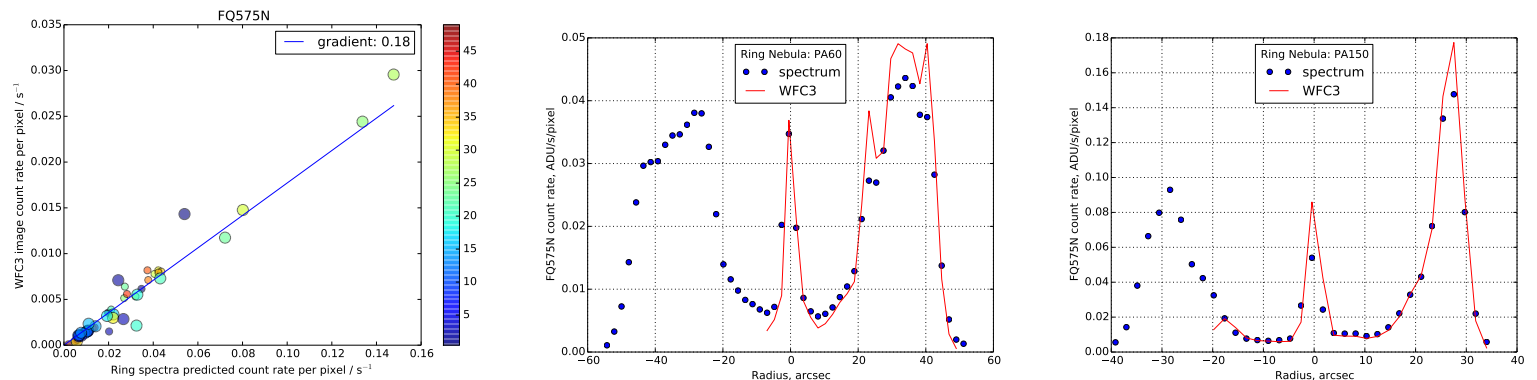


Fig. 20.— Ring Nebula raw filter comparison for FQ575N

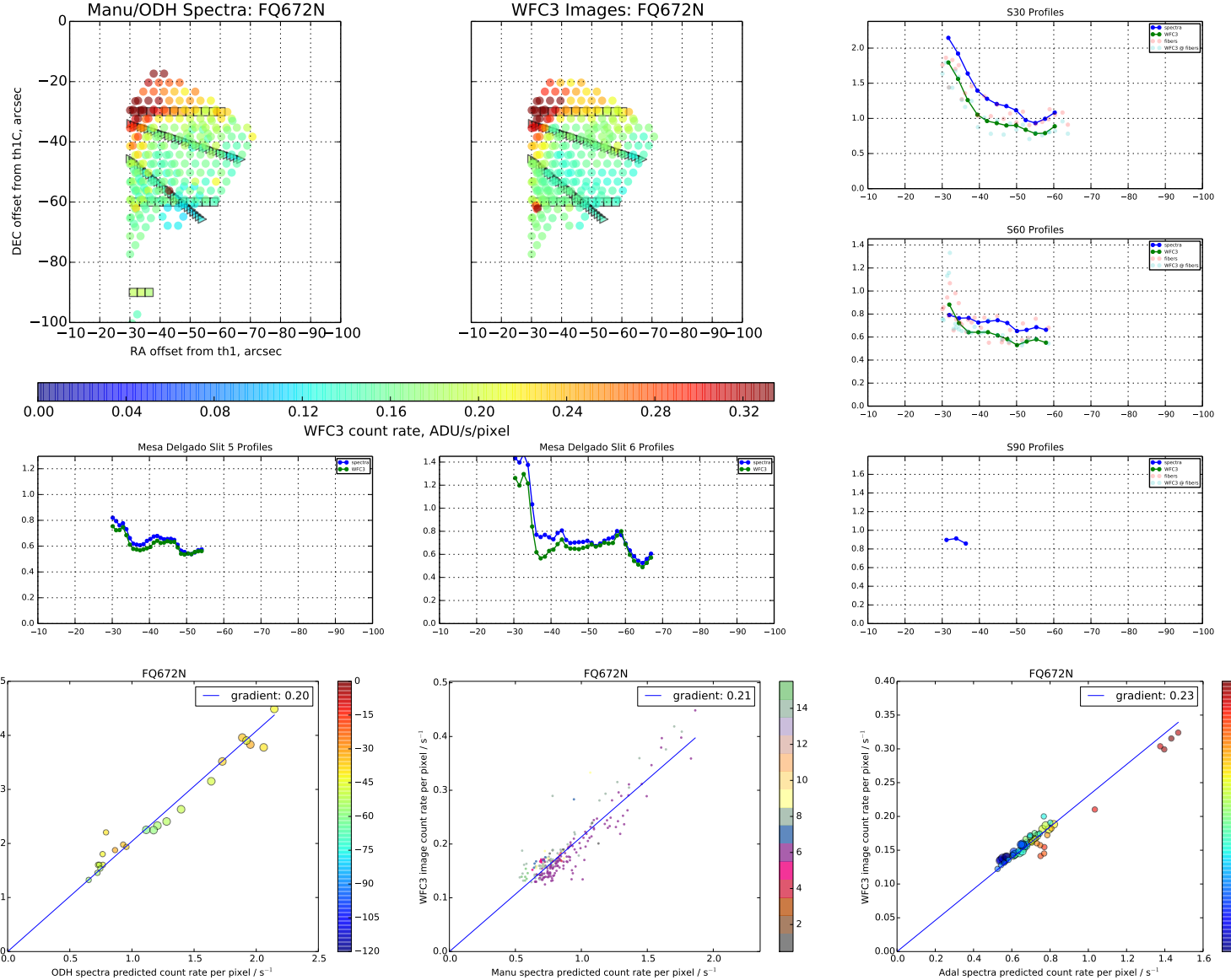


Fig. 21.— Orion Nebula raw filter comparison for FQ672N

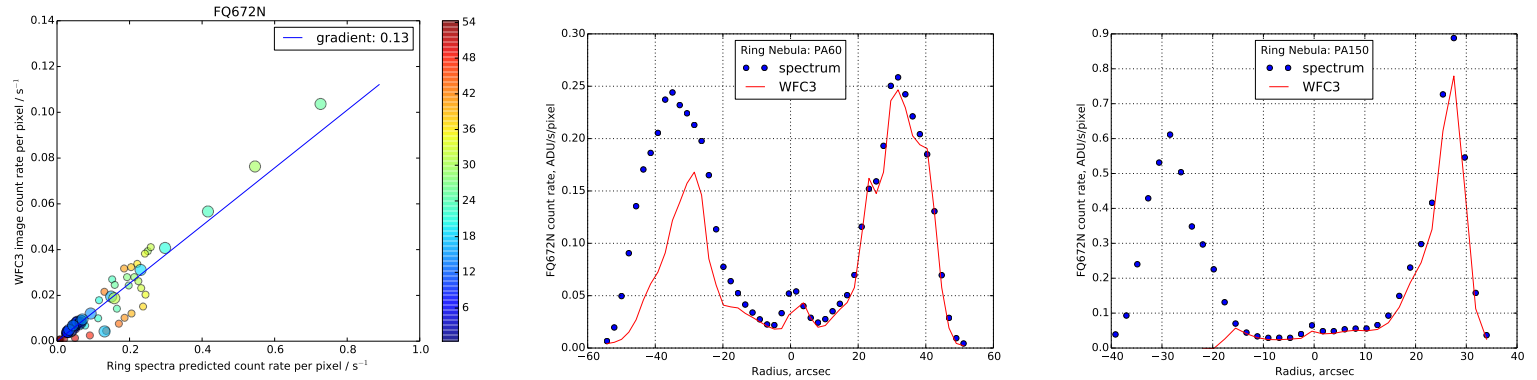


Fig. 22.— Ring Nebula raw filter comparison for FQ672N

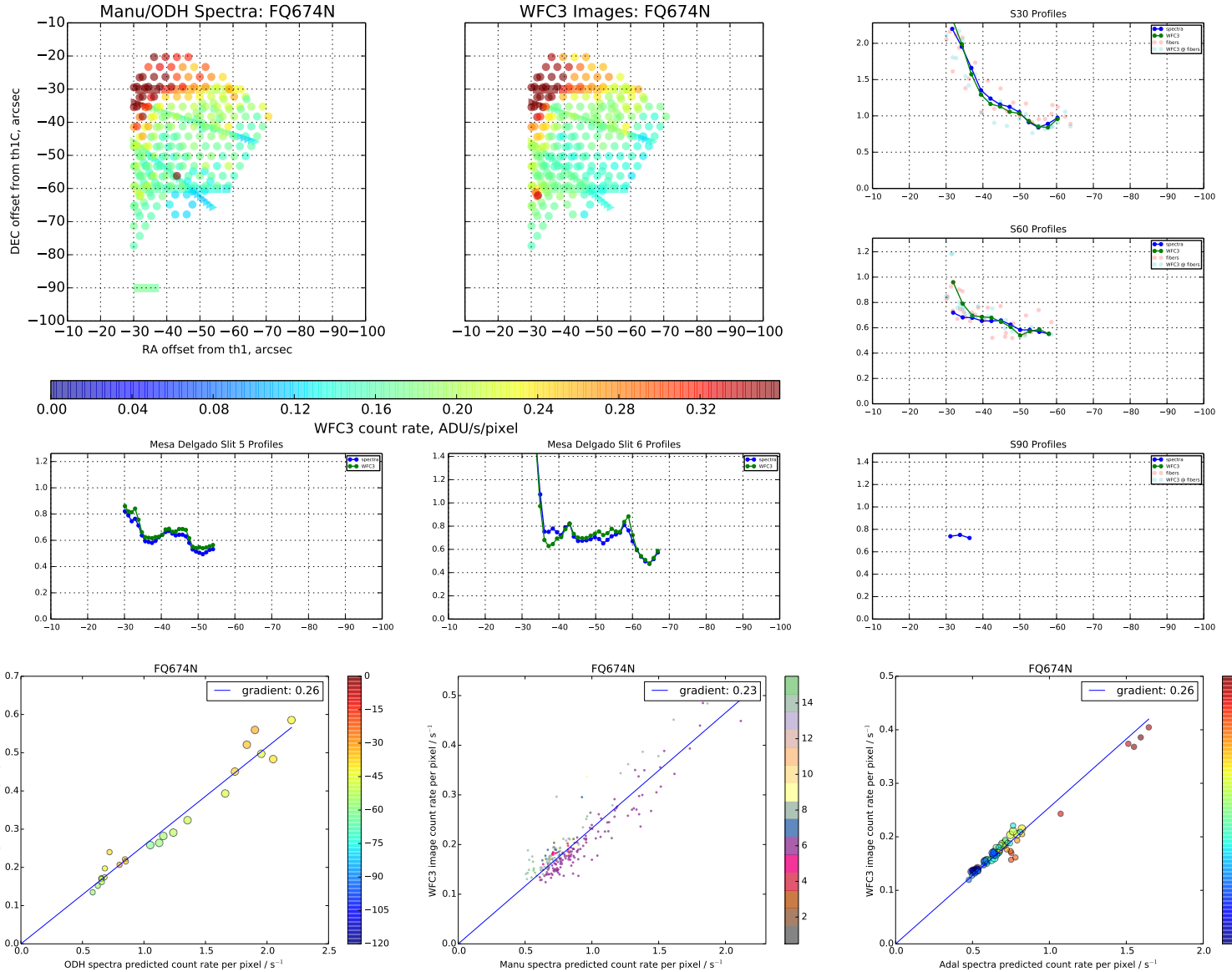


Fig. 23.— Orion Nebula raw filter comparison for FQ674N

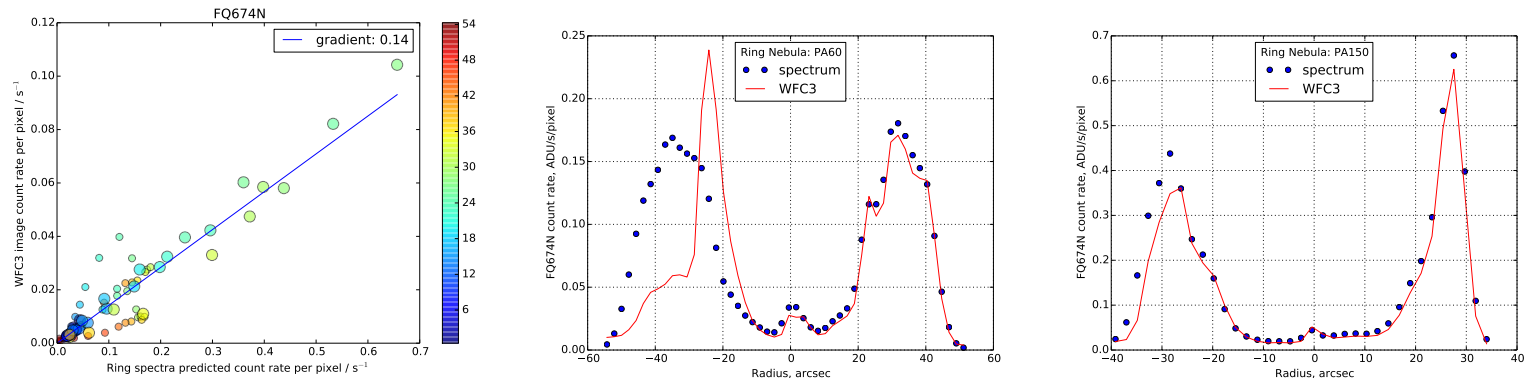


Fig. 24.— Ring Nebula raw filter comparison for FQ674N

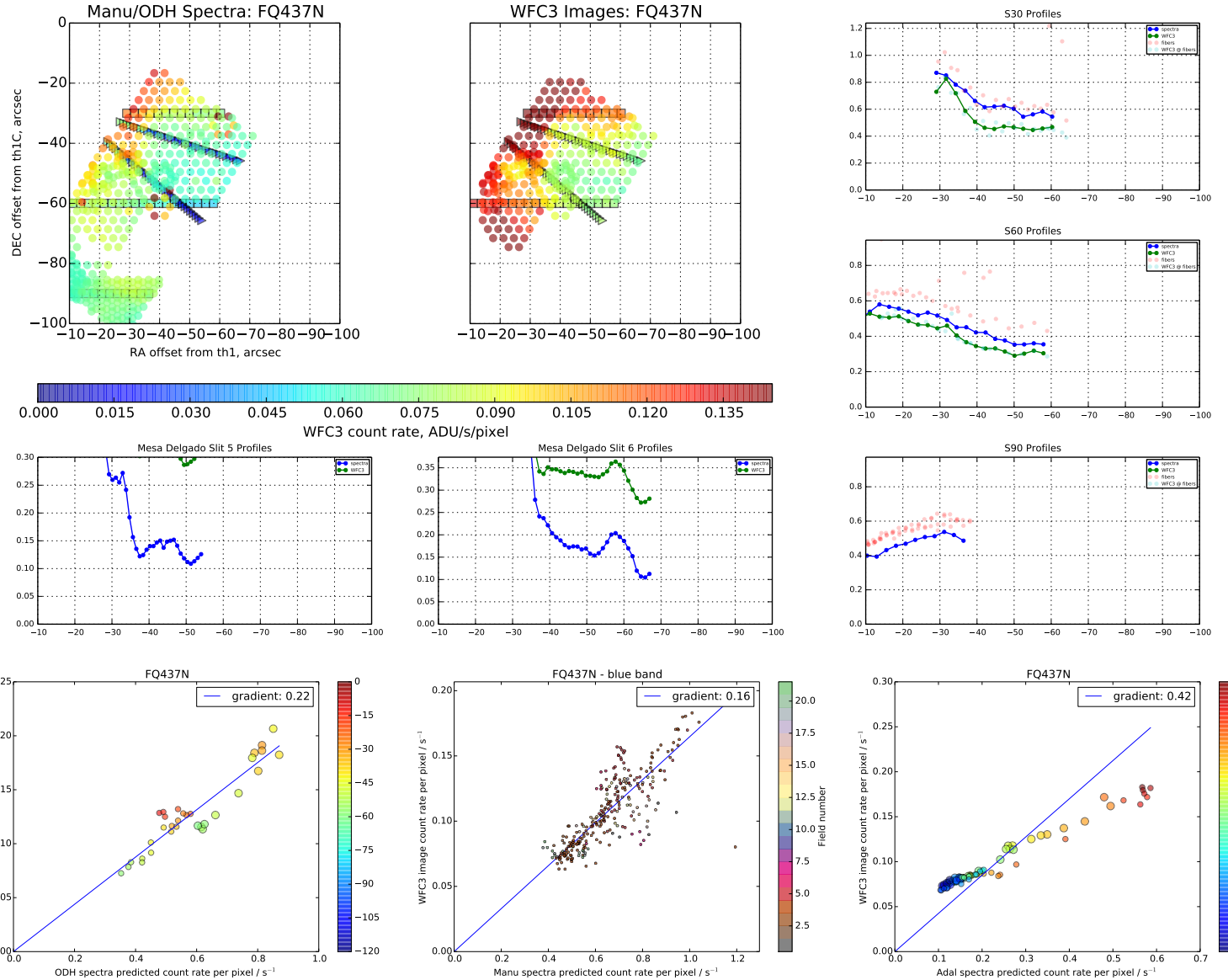


Fig. 25.— Orion Nebula raw filter comparison for FQ437N

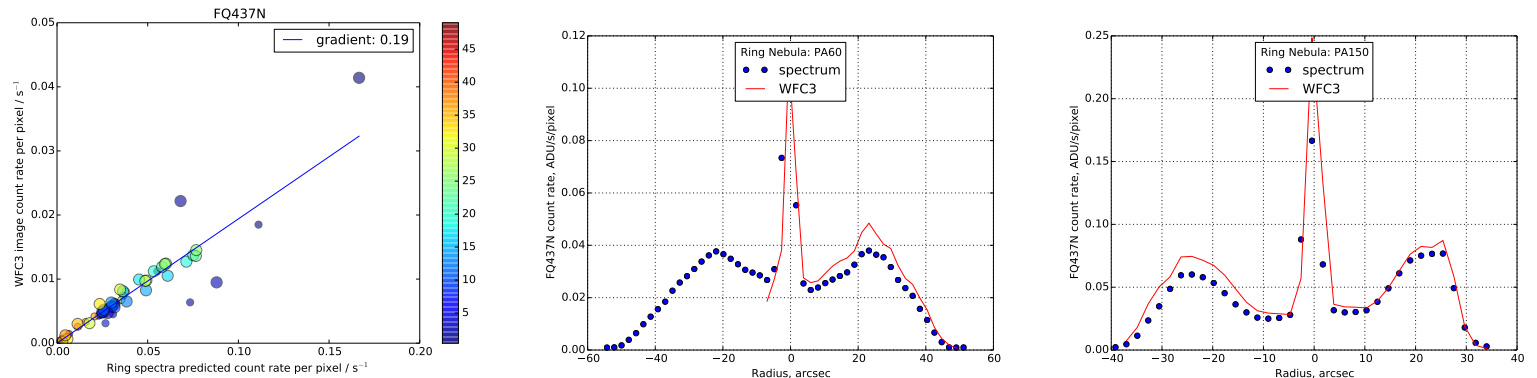


Fig. 26.— Ring Nebula raw filter comparison for FQ437N

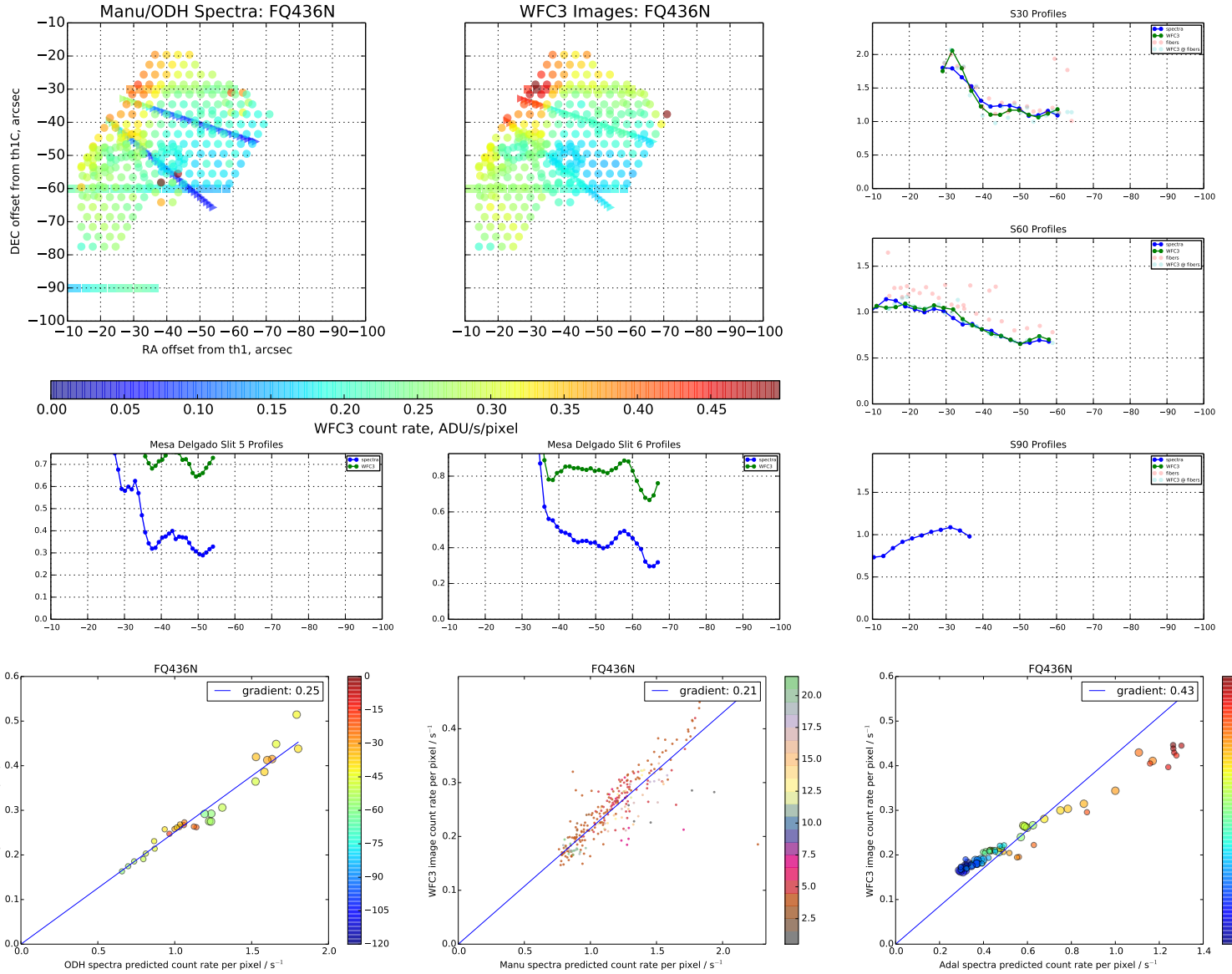


Fig. 27.— Orion Nebula raw filter comparison for FQ436N

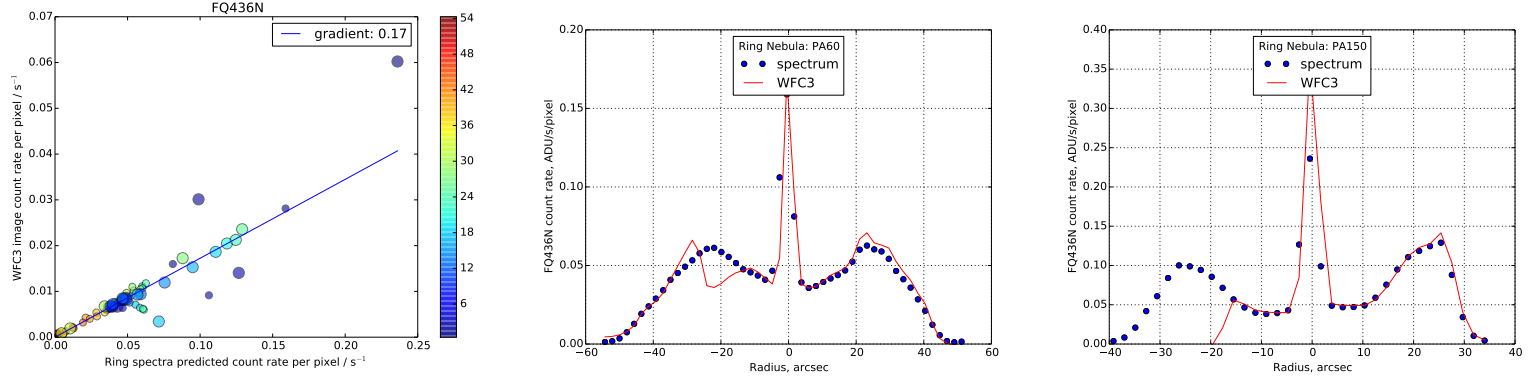


Fig. 28.— Ring Nebula raw filter comparison for FQ436N

REFERENCES

- Mesa-Delgado, A., Esteban, C., & García-Rojas, J. 2008, ApJ, 675, 389
- Núñez-Díaz, M., Mesa-Delgado, A., Esteban, C., López-Martín, L., García-Rojas, J., & Luridiana, V. 2012, MNRAS, 421, 3399
- O'Dell, C. R., Ferland, G. J., Henney, W. J., & Peimbert, M. 2013, AJ, 145, 92
- O'Dell, C. R., & Harris, J. A. 2010, AJ, 140, 985

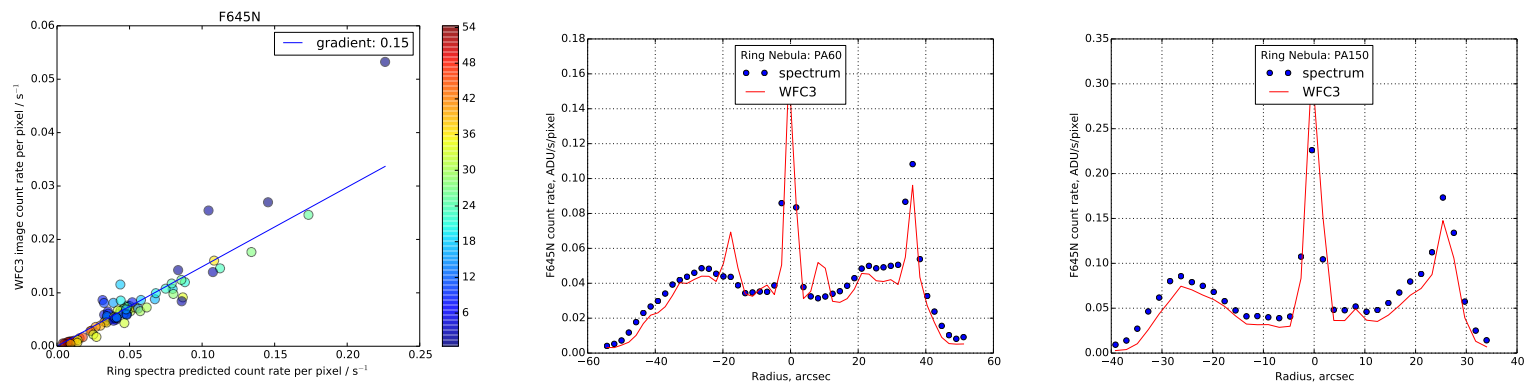


Fig. 29.— Ring Nebula raw filter comparison for F645N